READ 2024
RESEARCH & EDUCATION IN AIRCRAFT DESIGN
WARSAW, POLAND | 6-8 NOVEMBER 2024

AERODYNAMIC ANALYSIS OF HIGH-CAMBERED MORPHING AIRFOILS FOR MICRO UNMANNED AERIAL VEHICLES APPLICATIONS

Łukasz Kiszkowiak[1], Marta Marciniuk[2], Paweł Piskur[3], Łukasz Malicki[2], Katarzyna Strzelecka[2], Krzysztof Sibilski[4] & Stanisław Kachel[1]

[1] Military University of Technology, Faculty of Mechatronics, Armament and Aerospace
[2] Wrocław University of Science and Technology, Faculty of Mechanical and Power Engineering, Department of Cryogenics and Aerospace Engineering
[3] Polish Naval Academy of the Heroes of Westerplatte, Faculty of Mechanical and Electrical Engineering
[4] Warsaw University of Technology, Institute of Aeronautics and Applied Mechanics

Abstract

UAVs are the fastest developing branch of aviation these days. There are numerous ways to preserve a UAV landing manoeuvre, but the most difficult to land and most vulnerable to damages are UAVs without landing gear. Existing concepts of preserving landing manoeuvre with UAV without landing gear mainly focus on minimizing the impact force and loads overstressing the structure of the UAV. Experiments were performed in hydrodynamic tunnel on low Reynolds number using PIV method. Numerical simulations were conducted in two-dimensional domain with k-ω SST turbulence model. Results show lift force and drag coefficient increase with the increase of the angle of attack, for all geometries. The coefficients are increasing also with the camber increase. Authors created revolutionary concept combining perched landing method with morphing airfoils. This solution could not only contribute to minimizing the damage occurring to the UAV during landing, but also to improving the aerodynamic efficiency of the UAV during flight.

Keywords: morphing airfoil, UAV, Computational Fluid Dynamics, Particle Image Velocimetry, aerodynamics

1. Introduction

Morphing airfoils with variable camber are currently wide researched in terms of aerodynamic efficiency improvement of commercial aircraft [1]. The development of materials in the last few decades enabled researchers to conduct various technical solutions for morphing wings, allowing to create more revolutionary concepts [2]. Recently researchers started to examine morphing airfoils on micro UAVs and low Reynolds numbers. Majid and Jo [3] discovered morphing airfoils to increase aerodynamic efficiency of the wing by 18,7% comparing to wing with conventional mechanisation. UAVs are the fastest developing branch of aviation these days [4]. One of the difficulties UAVs are struggling with are landing methods, especially in rough terrain [5].
There are numerous ways to preserve UAV landing manoeuvre, but as it comes to micro UAVs without landing gear, all of these methods have disadvantages and are burdened with the risk of damaging aircraft [6]. One of the most popular methods is belly landing. The examples of such landing solution can be fixed-wing UAVs “Warmate” [7] or “FleEye” [8-9] from WB Electronics Group Company. “FleEye” also represents a group of observation UAVs. The observation head is placed underneath the fuselage to maximise the observation angle what causes difficulties during landing. Observation head can be easily damaged during belly landing manoeuvre. Net landing and hook recovery systems are commonly used on vessels [10]. On dry land these methods require specific equipment and generate logistic difficulties, especially in rough terrain. Also the approach is usually performed autonomously and during difficult weather conditions the aircraft can be easily pushed off the approach path and miss the recovery installation [5]. Common landing method is also parachute landing [11]. The parachute is mounted inside the fuselage of the micro UAV and is deployed before

touchdown ensuring lower impact with the ground. Its disadvantage is additional weight to the UAV which lowers the useful payload weight and less space for payload in the fuselage. An interesting landing method is perched landing or deep stall landing. University of Bristol presented a UAV with rotating wing. It rotates the wing during final approach without changing the angle of the fuselage and dramatically decreases the landing speed [12].
The authors of this work examined the fascinating ability of morphing airfoils to create drag in high-cambered stage. The target-aircraft was Micro Unmanned Aerial Vehicle (Micro UAV). Authors prepared six two-dimensional geometries, based on NACA24012 profile. The research was conducted both, numerically and experimentally. Both investigations were obtained in two-dimensional environment.

2. Materials and methods

2.1 Camber Morphing Airfoils

Based on NACA24012 airfoil, six airfoil geometries were generated. The front section of NACA24012 airfoil was fixed and only the back section varied in shape (Figure 1).

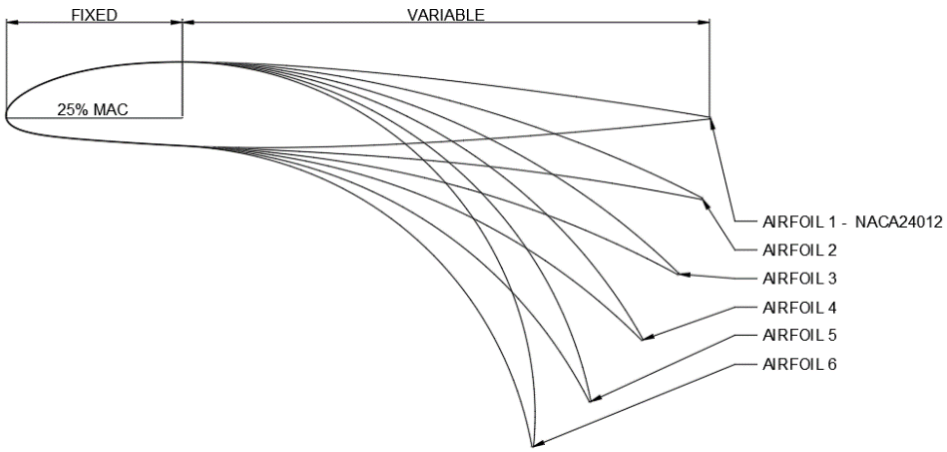

Figure 1. The visualisation of prepared geometries.

The chord lines are getting shorter with the increase of the camber. The initial angle of attack of the airfoils is also changing with the trailing edge deflection (Table 1), this is why authors use the expression “setting angle”, when referring to changing the angle of the geometries to the airflow.

Table 1. Parameters of prepared geometries.

Parameter	Airfoil					
	1	2	3	4	5	6
Chord length, mm	250	249	246	240	231	221
Initial angle of attack, °	0	7	13	19	26	32

From the two-dimensional geometries the three-dimensional models were created. The models were divided into pieces suitable for 3D printer, further printed using polylactic acid material (PLA). After printing the surface was processed to ensure the smooth surface for undisturbed by surface roughness flow.

2.2 Hydrodynamic Tunnel Experiments

The experiments were performed in the hydrodynamic tunnel of Military University of Technology in Warsaw. The hydrodynamic tunnel has a closed fluid circulation and is placed in a room with stable temperature and humidity. Its rectangular test section is 915 mm deep, 1830 mm long and 610 mm

wide [13-14]. The experiments were conducted using Particle Image Velocimetry method. The experimental setup (Figure 2) included high speed camera recording the glass particles with 10 μm diameter that were first added to water.

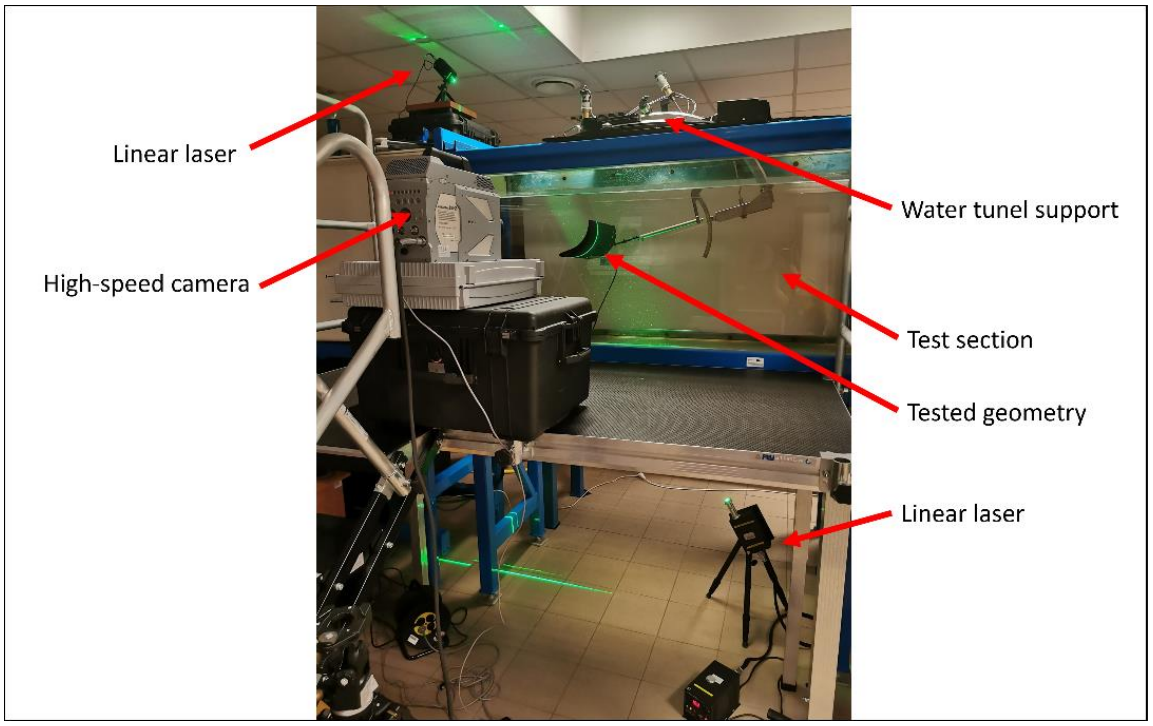

Figure 2. The experimental setup.

Two linear lasers enlightened the particles in one plane to minimise the shadow region. The models were painted to matt black colour to minimise the reflection. The flow parameters are presented in Table 2.

Table 2. Water flow parameters.

Parameter	Value
Water temperature	T = 26.3 °C
Kinematic viscosity	$v = 8.71 \cdot 10^{-7}$ m^2/s
Flow speed	v = 0.0762 m/s (3 in/s)
Reynolds number for Airfoil 1	Re = 21900

2.3 Mathematical Model and Numerical Simulations

Several scientific papers [15 - 19] show the possibilities of using numerical methods to obtain overall information about the aerodynamic characteristics of aircraft or their parts. Worth of mentioning is also, that such a method can be used in further design, starting from the influence of deflected control surfaces, influence of the propeller, and even the cooling systems of the engine and cabin could be tested [20, 21]. Also the armament drop safety can be tested [22] in order to avoid contact with the fuselage or other part of the aircraft. Flow simulations were conducted by solving the steady-state incompressible Navier–Stokes (1) and continuity equations (2). The study employed the Semi-Implicit Method for Pressure Linked Equations (SIMPLE) algorithm [23 – 25], along with the widely adopted k-ω shear stress transport (SST) turbulence model [26 – 28]. The convective form of the steady-state k-ω SST model is represented by equations (3) and (4) [29].

$$(\mathbf{u} \cdot \nabla)\mathbf{u} = -\nabla(p/\rho) + \nu\nabla 2\mathbf{u} \tag{1}$$

$$\nabla \cdot \mathbf{u} = 0 \tag{2}$$

$$\nabla \cdot (\mathbf{u}k) = \frac{P}{\rho} - \beta^* \omega k + \nabla \cdot [(\nu + \sigma_k \nu_t)\nabla k] \quad (3)$$

$$\nabla \cdot (\mathbf{u}\omega) = \frac{\gamma}{\mu_t} P - \beta\omega^2 + \nabla \cdot [(\nu + \sigma_\omega \nu_t)\nabla\omega] + 2(1 - F_1)\frac{\sigma\omega_2}{\omega}\nabla k \nabla\omega \quad (4)$$

where $\mathbf{u} = (u_x, u_y)$ is the fluid velocity vector, ρ is the fluid density, p is pressure, k is the turbulent kinetic energy, ω is the specific dissipation rate, μ_t is the turbulent eddy viscosity, v is the kinematic viscosity, ν_t is the turbulent kinematic viscosity, σ_k is the turbulent Prandtl number for k, σ_ω is the turbulent Prandtl number for ω, P is the production term, and F_1 is the blending function [30].

The aforementioned equations were discretized using the Finite Volume Method (FVM), and the simulations were carried out using OpenFOAM, an open-source C++ toolbox [31 – 33]. Figure 3 shows the conceptual layout of the computational domain, with the distances and dimensions indicated.

The numerical studies modelled the 2D hydrodynamics around the airfoil geometries under steady-state conditions. A summary of the flow characteristics is presented in Table 3.

The convergence criterion for steady-state simulations utilized residual control for velocity $u_x|u_y \leq 1 \times 10^{-6}$, kinematic pressure $p \leq 1 \times 10^{-6}$, turbulent kinetic energy, and the specific dissipation rate $k|\omega \leq 1 \times 10^{-6}$. A backup convergence criterion was set at a total number of iterations $n = 35000$.

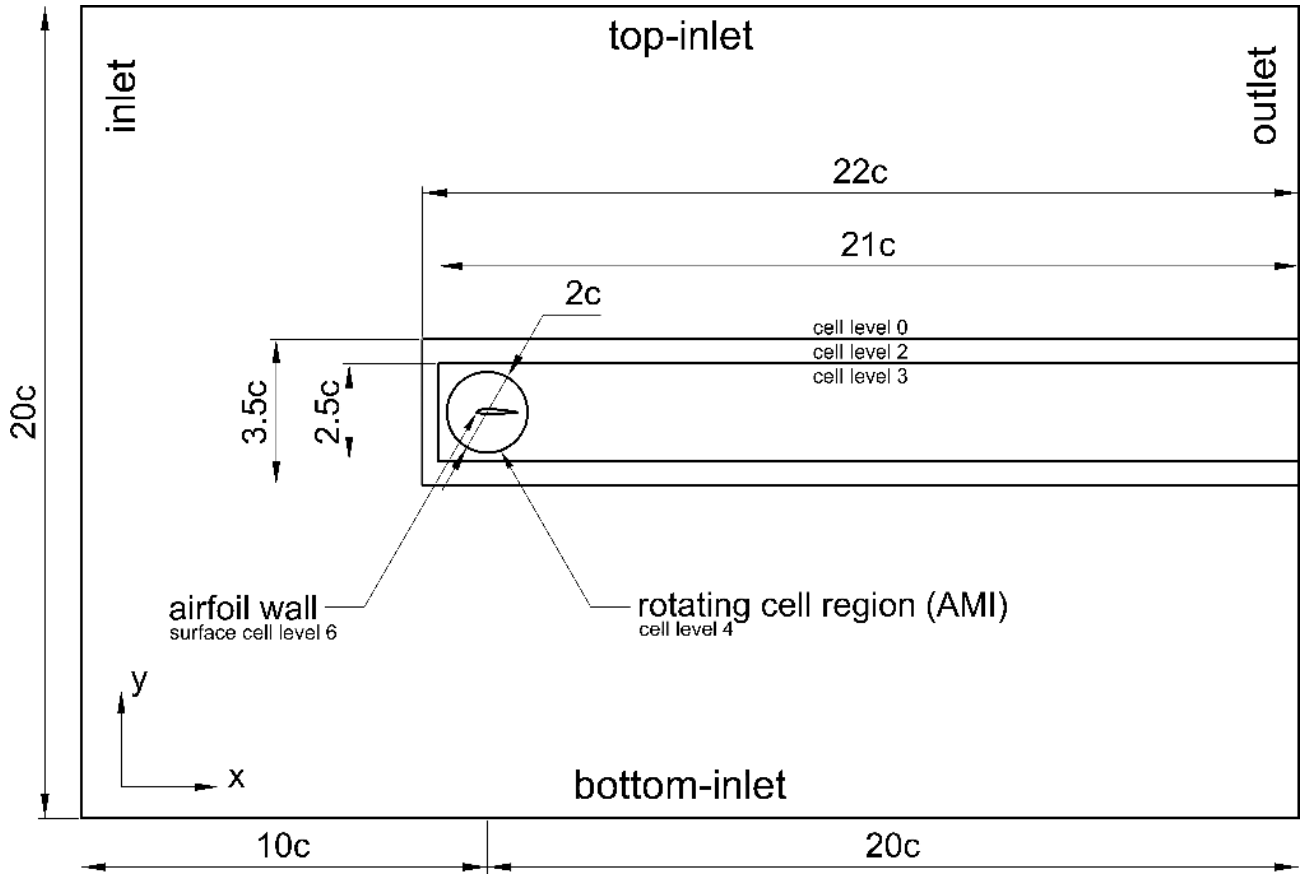

Figure 3. Computational domain.

Table 3. Flow characteristics.

Parameter	Value
Type	steady-state 2D incompressible flow
Fluid	Newtonian, single-phase
Material	water at 26.3°C
Water density	$\rho = 996.784\ \mathrm{kg/m^3}$
Kinematic viscosity	$\upsilon = 8.71 \times 10^{-7}\ \mathrm{m^2/s}$
Reynolds number	$\mathrm{Re} = 19400 - 21900$
Far-field flow speed	$\mathbf{u} = 0.0762\ \mathrm{m/s}$
Airfoil chord range	$c = 0.231 - 0.250\ \mathrm{m}$

3. Results

From experimental PIV approach velocity distribution was obtained. The results were the average values from 500 frames. They were used as a validation for numerical simulations. Numerical results were discrete values from one iteration. This is why the presented figures are not identical, but the similarities are clearly visible and the results are comparable. In general it can be noted that CFD results present slightly higher velocity especially above the cambered airfoils and behind the trailing edge. Representative graphic results were presented in Figures 4 and 5.

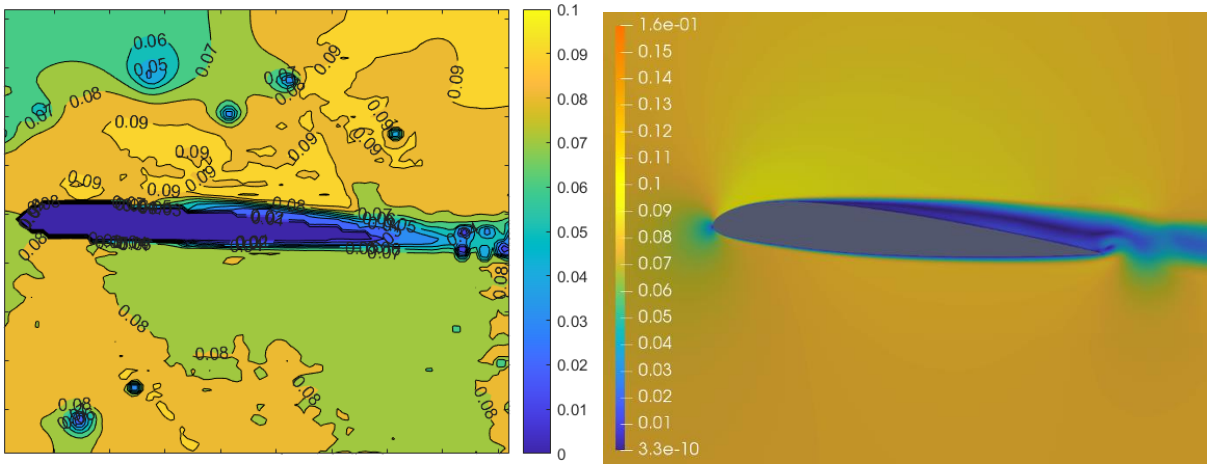

Figure 4. Velocity distribution for Airfoil 1 geometry and setting angle 4°. PIV result (left) and CFD result (right).

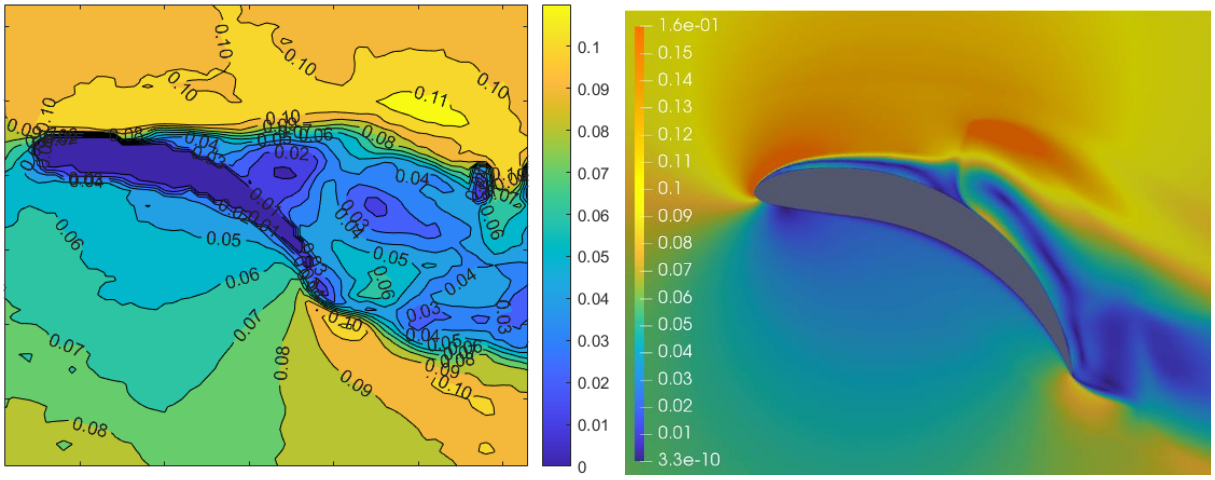

Figure 5. Velocity distribution for Airfoil 5 geometry and setting angle 4°. PIV result (left) and CFD result (right).

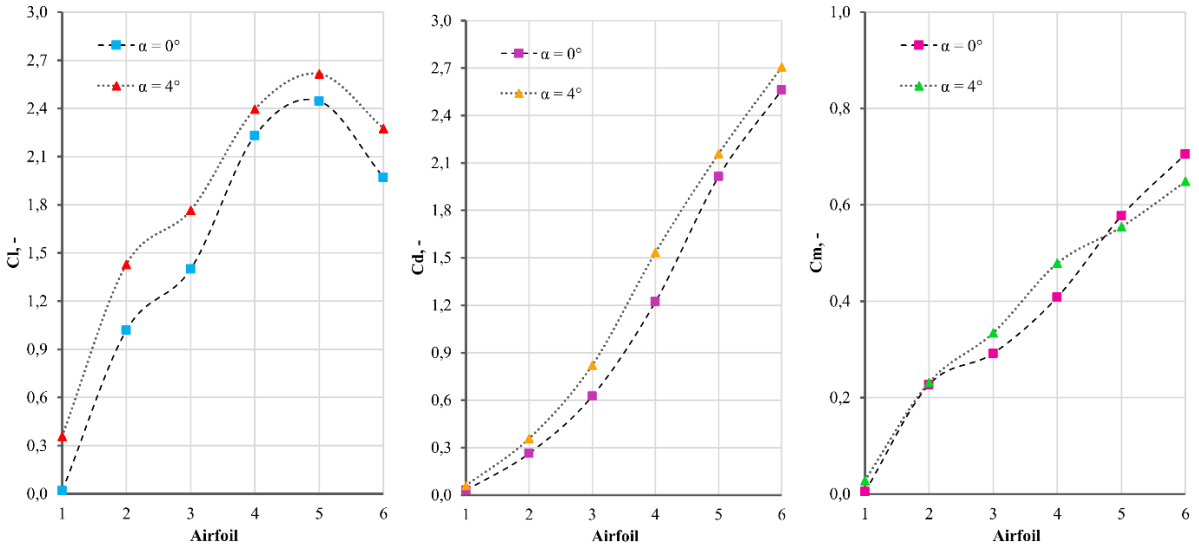

Figure 6. Characteristic of lift force coefficient (left), drag coefficient (middle) and pitching moment coefficient (right) for each airfoil geometry and two setting angles.

From numerical simulations coefficients characteristics were obtained. The characteristics (Figure 6) present lift force, drag and pitching moment changes with the camber increase for two setting angles.

Lift force coefficient increases with the camber increase except the highest-cambered airfoil (Airfoil 6). Increasing the setting angle increases the lift coefficient values for every airfolil geometry. Drag coefficient increases significantly with the increase of the camber and setting angle. The characteristics show the potential of high-cambered airfoils to create drag. The last characteristic presents the pitching moment coefficient for each airfoil geometry. Pitching moment coefficient also increases with the increase of trailing edge deflection. Interesting is, that the pitching moment coefficient is lower for high-cambered airfoils at higher setting angle.

4. Conclusions

Micro UAVs are an excellent solution for supporting human missions in a variety of environments. As the most dangerous phase of the UAV flight is the landing phase, the authors created a revolutionary morphing airfoil design that could reduce the overall damage of the UAVs during landing and increase the aerodynamic efficiency of the aircraft. The results show the change of the lift force, drag and pitching moment coefficients with the change of the airfoil camber. Two setting angles were selected to demonstrate the influence of the camber morphing on the coefficient characteristics change. Lift force coefficient increases for nearly every geometry, but setting angle increase shows constant impact on lift force coefficient values. Drag coefficient significantly increases with the increase of the camber and setting angle.

Results show promising ability of the morphing airfoils to create drag in high-cambered stage. Low morphing stages of the airfoil could be utilized during take-off manoeuvres like conventional flaps, while high morphing stages are considerable solution for Micro UAV's during landing phase, especially in rough terrain. Higher drag force during last phase of landing manoeuvre could provide lower speed during touchdown and lower risk of damaging the aircraft structure.

5. Contact Author Email Address

Łukasz Kiszkowiak; mailto: lukasz.kiszkowiak@wat.edu.pl

6. Copyright Statement

7. Funding

The paper was elaborated basing on data obtained during the research carried out in the following project:

- A multi-sensor platform for imaging and detecting threats occurring in areas with high dynamics of changes in environmental conditions- DOB-SZAFIR/01/B/038/04/2021– funded by the National Centre for Research and Development;

that was implemented in the Military University of Technology.

References

[1] Moens, Frédéric "Augmented aircraft performance with the use of morphing technology for a turboprop regional aircraft wing." Biomimetics 4.3 (2019): 64.

[2] Ahmad, Dilshad, and Rafic M. Ajaj. "A multiaxial fracture of ecoflex skin with different shore hardness for morphing wing application." Polymers 15.6 (2023): 1526.

[3] Majid, Tuba, and Bruce W. Jo. "Comparative aerodynamic performance analysis of camber morphing and conventional airfoils." Applied Sciences 11.22 (2021): 10663.

[4] Faiyaz Ahmed, JC Mohanta, Anupam Keshari, and Pankaj Singh Yadav. Recent advances in unmanned aerial vehicles: a review. Arabian Journal for Science and Engineering, 47(7):7963–7984, 2022.

[5] Guillaume Jouvet, Yvo Weidmann, Eef Van Dongen, Martin P Lüthi, Andreas Vieli, and Jonathan C Ryan. High-endurance uav for monitoring calving glaciers: Application to the inglefield bredning and eqip sermia, greenland. Frontiers in Earth Science, 7:206, 2019.

[6] Marta Marciniuk, Paweł Piskur, Łukasz Kiszkowiak, Łukasz Malicki, Krzysztof Sibilski, Katarzyna Strzelecka, Stanisław Kachel, and Zygmunt Kitowski. Aerodynamic analysis of variable camber-morphing airfoils with substantial camber deflections. Energies, 17(8):1801, 2024.

[7] https://www.wbgroup.pl/produkt/system-amunicji-krazacej-warmate/, WB Group Warmate, access: 08.2024.

[8] https://www.wbgroup.pl/produkt/bezzalogowy-system-powietrzny-klasy-mini-flyeye/, WB Group FlyEye, access: 08.2024.

[9] https://www.wbgroup.pl/app/uploads/2017/06/flyeye_eng_large_21q03.pdf, WB Group FlyEye, access: 08.2024.

[10] Zhu, Yongchao, et al. "Research on recovery technology of ship-borne fixed-wing UAV." Third International Conference on Mechanical, Electronics, and Electrical and Automation Control (METMS 2023). Vol. 12722. SPIE, 2023.

[11] https://manta-air.com/uav_safety_and_recovery_systems/, UAV Safety & Recovery, access: 08.2024.

[12] https://newatlas.com/drone-perch-uav-landing-bristol-university/47349/, Fixed-wing drone learns to land like a bird, access: 08.2024.

[13] Kerho, M., and B. Kramer. "Five-component balance and computer-controlled model support system for water tunnel applications." Rolling Hills Research Corporation (RHRC): El Segundo, CA, USA (2009).

[14] Animus, R. H. R. C. "Research water tunnel specification." El Segundo California, User's Manual (2009).

[15] Goetzendorf-Grabowski T., Kwiek A. Study of the impact of aerodynamic model fidelity on

the flight characteristics of unconventional aircraft. Applied Sciences, 13(22), 2023.
[16] Kwiek A., Figat M., Goetzendorf-Grabowski T. The study of selected aspects of the suborbital vehicle return flight trajectory. Aerospace, 10(5), 2023.
[17] Aleksander Olejnik, Łukasz Kiszkowiak, Piotr Zalewski, and Adam Dziubiński. Low-cost satellite launch system - aerodynamic feasibility study. Aerospace, 9(6), 2022.
[18] Halila G.L.O., Antunes A. P., Ricardo Galdino da Silva, João Luiz F. Azevedo, (2019), Effects of boundary layer transition on the aerodynamic analysis of high-lift systems, Aerospace Science and Technology, Vol. 90, 233-245, https://doi.org/10.1016/j.ast.2019.04.051
[19] A. Viviani, A. Aprovitola, G. Pezzella, C. Rainone, (2020), CFD design capabilities for next generation high-speed aircraft, Acta Astronaut, Vol.178, 143-158, https://doi.org/10.1016/j.actaastro.2020.09.006
[20] Goetzendorf-Grabowski, T. (2023), Flight dynamics of unconventional configurations, Progress in Aerospace Sciences, Vol. 137, 100885, https://doi.org/10.1016/j.paerosci.2023.100885
[21] Zdobysław Goraj, Andrzej Frydrychewicz, Stanislaw Danilecki, Aleksander Olejnik, and Łukasz Kiszkowiak. Conceptual design of a third generation aerobatic aircraft. Proceedings of the Institution of Mechanical Engineers, Part G: Journal of Aerospace Engineering, 237:095441002211363, 11 2022.
[22] Aleksander Olejnik, Adam Dziubiński, and Łukasz Kiszkowiak. Separation safety analysis using CFD simulation and remeshing. Aerospace Science and Technology, 106:106190, 2020.
[23] OpenFOAM: User Guide—simpleFOAM. Available online: https://www.openfoam.com/documentation/guides/latest/doc/guide-applications-solvers-incompressible-simpleFoam.html, access: 10.2024.
[24] Steady-State Solution. Available online: https://doc.cfd.direct/notes/cfd-general-principles/steady-state-solution, access: 10.2024.
[25] The SIMPLE Algorithm in OpenFOAM. Available online: https://openfoamwiki.net/index.php/OpenFOAM_guide/The_SIMPLE_algorithm_in_OpenFOAM, access: 11.2024.
[26] K-Omega Turbulence Models. Available online: https://www.simscale.com/docs/simulation-setup/global-settings/k-omegasst/, access: 10.2024.
[27] Menter, F. Zonal two equation kw turbulence models for aerodynamic flows. In Proceedings of the 23rd fluid dynamics, plasmadynamics, and lasers conference, Moffett Field, CA, USA, 6–9 July 1993; p. 2906.
[28] Menter, F.R. Two-equation eddy-viscosity turbulence models for engineering applications. AIAA J. 1994, 32, 1598–1605.
[29] The Menter Shear Stress Transport Turbulence Model. Available online: https://turbmodels.larc.nasa.gov/sst.html, access: 10.2024.
[30] Andersson, B.; Andersson, R.; Hakansson, L.; Mortensen, M.; Sudiyo, R.; Van Wachem, B. Computational Fluid Dynamics for Engineers; Cambridge University Press: Cambridge, UK, 2011.
[31] About OpenFOAM. Available online: https://cfd.direct/openfoam/about/, access: 10.2024.
[32] OpenFOAM Overview. Available online: https://www.openfoam.com/governance/overview, access: 11.2024.
[33] OpenFOAM History. Available online: https://openfoam.org/company-history/, access: 10.2024.